REGULAR PAPER

Optimum waveguide-core size for reducing device property distribution of Si-wire waveguide devices

Japanese Journal of Applied Physics **54**, 04DG03 (2015) **REGULAR PAPER**
http://dx.doi.org/10.7567/JJAP.54.04DG03

Optimum waveguide-core size for reducing device property distribution of Si-wire waveguide devices

Munetoshi Soma[1], Tomohiro Kita[1]*, Yuichiro Tanushi[1], Munehiro Toyama[1,2], Miyoshi Seki[2], Nobuyuki Yokoyama[2], Minoru Ohtsuka[2], and Hirohito Yamada[1]

[1]*Department of Communications Engineering, Tohoku University, Sendai 980-8579, Japan*
[2]*National Institute of Advanced Industrial Science Technology (AIST), Tsukuba, Ibaraki 305-8569, Japan*
E-mail: tkita@ecei.tohoku.ac.jp

Received September 10, 2014; accepted November 26, 2014; published online March 6, 2015

We investigated the waveguide-core size distribution of ring resonators fabricated on a 300 mm silicon-on-insulator (SOI) wafer using a CMOS-compatible process featuring ArF immersion lithography. These ring resonators were constructed in a Si-wire waveguide with a standard core size of 400 nm width and 220 nm height. The group refractive indices of the waveguide were derived from the transmission spectra of the ring resonators. From the deviation of these group refractive indices, the waveguide-core width distribution was estimated to be 5 nm, and the waveguide-core height distribution was estimated to be 1 nm. Moreover, the device property distribution of various Si-wire waveguide depended on the estimated fabrication error was calculated. The waveguide core with the smallest device property distribution had a 540 nm width and a 160 nm height, and this waveguide has a device property distribution of 2/3 value compared with the standard core size.

1. Introduction

Silicon photonics is attractive for use in fabricating various photonic devices or integrated circuits on large-scale wafers using complementary metal oxide semiconductor (CMOS) compatible processes.[1,2] It has been actively investigated for various applications such as optical interconnect devices[3–8] and large-capacity optical communication.[9–15] Recently, 300 mm silicon-on-insulator (SOI) wafers have been used for fabricating Si photonic devices.[16–24] The uniformity of the properties of Si photonic devices formed on such large wafers is a key issue in producing photonic devices or integrated circuits with a high efficiency. The device property uniformity of individual photonic devices has already been investigated.[16–18,25–28]

This research entails both experimental and theoretical studies. In Sect. 2, we fabricated Si-wire patterns and ring resonators on a 300 mm SOI wafer using ArF immersion lithography. We then addressed the uniformity of the Si-wire core size as well as the uniformity of the process. The distribution of the Si-wire width on a wafer was measured using critical-dimension scanning electron microscopy (CD-SEM). We measured the transmission spectra of ring resonators, which were used to derive the group refractive indices (n_g) of the waveguide. By comparing the deviation of the measured n_g and finite element method (FEM) calculation results, we experimentally clarified the distribution of the waveguide-core size fabricated by current processes.

In Sect. 3, assuming that the estimated waveguide-core size distribution arises for waveguides of any core size, we obtained the relationship between the effective refractive index (n_{eff}) distribution and the waveguide-core size using FEM calculation. From this result, we theoretically determined the waveguide-core size with a minimum n_{eff} distribution and a high n_{eff}. Because n_{eff} is an important parameter for determining device properties, minimizing the n_{eff} distribution leads to a reduced distribution of device properties. Therefore, we can improve the uniformity of Si-wire waveguide devices not only by improving semiconductor processes but also by optimizing the waveguide-core size.

2. Line width distribution on a wafer

2.1 Device fabrication process

In this section, we experimentally estimated the waveguide-core size distribution by measuring Si-wire patterns and ring resonators. Firstly, we fabricated 100-nm-wide Si-wire patterns and ring resonators with a 400-nm-wide Si-wire waveguide on a 300 mm SOI wafer with a 220-nm-thick SOI layer and a 2-μm-thick buried oxide (BOX) layer. We used an SOI wafer with less than 1 nm (3σ) thickness deviation in the SOI layer. For the fabrication process, a Si nitride (SiN) film was deposited by low-pressure chemical vapor deposition (LPCVD) as a hardmask for the subsequent SOI layer etching process. Then spin-on glass and spin-on carbon films were coated as antireflection layers for lithography. After coating with a photoresist, the waveguide patterns were defined using ArF immersion lithography. ArF immersion lithography consists of the CMOS 45 nm process and we have developed a less than 100 nm resolution for silicon photonics with any angle device feature by optimizing the illumination and resist properties. The device patterns were transferred to the SiN and SOI layers by inductively coupled plasma reactive-ion etching (ICP-RIE) with a HBr–Cl_2–O_2 gas mixture. Then the SiN hardmask was removed with hot phosphoric acid. Finally, a 2-μm-thick SiO_2 layer was deposited by tetraethoxysilane (TEOS) LPCVD as an over cladding layer. Waveguide samples were diced and polished on their end surfaces for optical coupling with an optical fiber for measurement.

Figure 1 shows the cross section of the Si-wire waveguide. The fabricated waveguides were buried channel waveguides with a height of 220 nm. The uniformity of the fabrication process on the wafer was investigated by the width measurement of the 100-nm-wide Si-wire patterns using CD-SEM. Figure 2 shows a contour map of the measured distribution of Si-wire widths on the wafer. The number of measurement points is 84; the average and 3σ deviation of the measured widths are 100.6 and 5.3 nm, respectively. The measured width is the bottom width of the waveguide cross section.

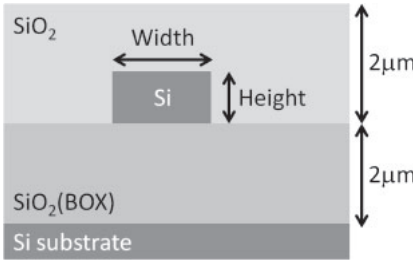

Fig. 1. Cross-sectional structure of Si-wire optical waveguides.

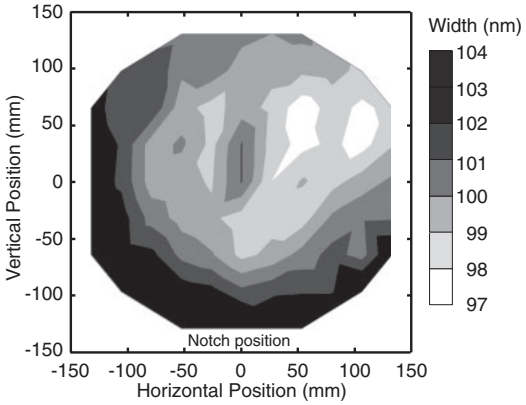

Fig. 2. Contour map of the widths of the fabricated 100-nm-wide Si-wire patterns at 84 points on the 300 mm SOI wafer. The average and 3σ deviation of measured widths are 100.6 and 5.3 nm, respectively.

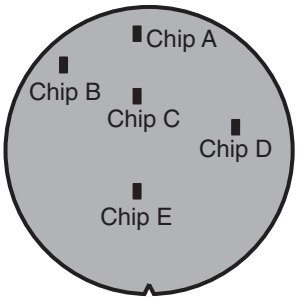

Fig. 3. Location of the small chips including measured ring resonator on a 300 mm SOI wafer.

2.2 Deviation of group refractive index

To examine the variation in the properties of Si-wire waveguide devices, we selected five chips from different positions on the wafer, as shown in Fig. 3. The chips were $6.5 \times 16\,\text{mm}^2$ and included ring resonators with the same device parameters. The distances from the wafer center to each of the chip centers were 126, 129, 52, 94, and 43 mm for chips A, B, C, D, and E, respectively. Figure 4 shows the structure of the fabricated race track type ring resonators. We selected a 400-nm-wide × 220-nm-high (Structure A) Si-wire waveguide as a common waveguide-core size, with a ring radius of 30 μm, a gap width between the ring and the busline waveguide of 0.3 μm, and a coupling length of 4.75 μm. To measure the transmission property of ring resonators, a tunable-wavelength laser (Santec TSL-210) with a wavelength range between 1540 and 1560 nm was used as the light source. The polarization of light inputted to the device was set to a transverse electric (TE)-like mode

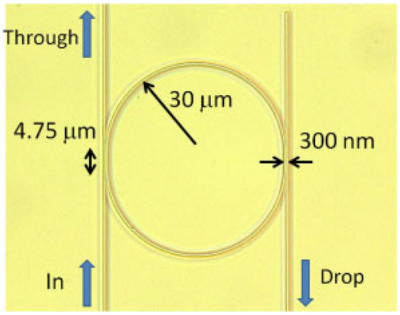

Fig. 4. (Color online) Top view of optical microscopy image of fabricated ring resonator. The ring radius, gap between the ring and the busline waveguide, and coupling length are 30, 0.3, and 4.75 μm, respectively.

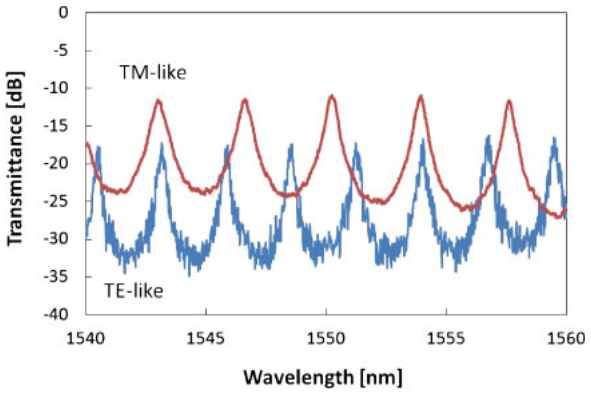

Fig. 5. (Color online) Drop spectrum of a ring resonator fabricated on Chip A.

or a transverse magnetic (TM)-like mode. The light was focused on the ring resonators using a lensed optical fiber. The light outputted from the drop port of the ring resonators was collected using another lensed optical fiber and the output light power measured using an optical power meter (Advantest Q8221).

Figure 5 shows an example of the transmission spectrum for the drop port of the ring resonator on chip A. The blue line shows the transmission spectrum measured in the TE-like mode, and the red line represents that in the TM-like mode. The resonance peak wavelength and free spectral range (FSR) were carefully estimated from the measured spectra by fitting them with Lorentzian functions. The n_g of the Si-wire waveguide can be estimated from the FSR using

$$n_g = \frac{\lambda^2}{\text{FSR} \cdot L_{\text{ring}}}, \tag{1}$$

where λ is the resonance peak wavelength and L_{ring} is the circumference of the ring with a designed value of about 200 μm. Figure 6 shows the wavelength dependence of the n_g of the Si-wire waveguide derived from the transmission spectra of ring resonators. The broken lines in Fig. 6 show n_g calculated by FEM calculation. The measured n_g values are slightly higher than the calculation results owing to the difference in cross-sectional core shape (we assumed that the Si core has a perfect rectangle shape from the FEM calculation, but the fabricated Si core is slightly trapezoidal) and uses the material refractive index data from the FEM calculation. The n_g of each device at a wavelength of

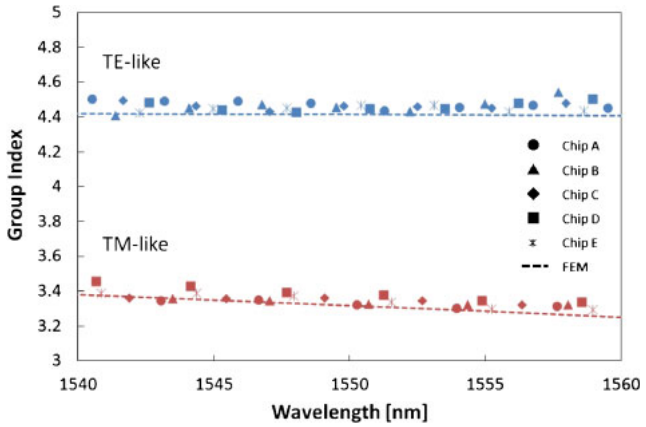

Fig. 6. (Color online) n_g of Si-wire waveguides derived from drop spectra of ring resonators. Broken lines show the calculated results of the waveguide structure.

1550 nm was calculated by linear approximation. The calculated n_g values ranged from 4.449 to 4.474 for the TE-like mode and from 3.330 to 3.389 for the TM-like mode; the maximum deviations from the average are less than 0.3% for the TE-like mode and 1.1% for the TM-like mode.

2.3 Distribution of waveguide-core size

The waveguide-core size distribution was estimated from the calculated n_g deviation shown in the preceding paragraph. We calculated this relationship by numerical simulation using FEM. In the FEM calculation, the wavelength dependences of the refractive indices of Si and SiO_2 materials were taken into consideration.[29] The n_g deviation can be calculated using

$$n_g \text{ deviation}(W, H) = \frac{n_g(W, H) - n_g(400, 220)}{n_g(400, 220)} \times 100. \quad (2)$$

Figure 7(a) shows the calculated n_g deviation for the TE-like mode and Fig. 7(b) shows that for the TM-like mode, both at a wavelength of 1550 nm. The n_g deviation seems to have a strong dependence on the waveguide-core width for the TE-like mode, but it certainly has a strong dependence on the waveguide-core height for the TM-like mode. The waveguide-core size dependence of n_g is different from that of the n_{eff}, because n_g is strongly affected by both material dispersion and waveguide structure dispersion. The waveguide-core size marked by a black broken line is for Structure A. The white areas on the color maps in Figs. 7(a) and 7(b) correspond to the n_g deviations derived from the transmission spectra of the ring resonators. Although these areas are widely distributed for each mode, the estimated waveguide-core size distributions should be the same for both modes. Therefore, the implicit intersection of these white areas shows the waveguide-core size distribution.[30] By the above method, the estimated maximum distribution of the waveguide-core width was 5 nm, and the waveguide-core height was 1 nm. These distribution values are in agreement with the measured result for Si-wire patterns.

3. Waveguide-core size with minimized device property distribution

In Sect. 2, we estimated the waveguide-core size distribution

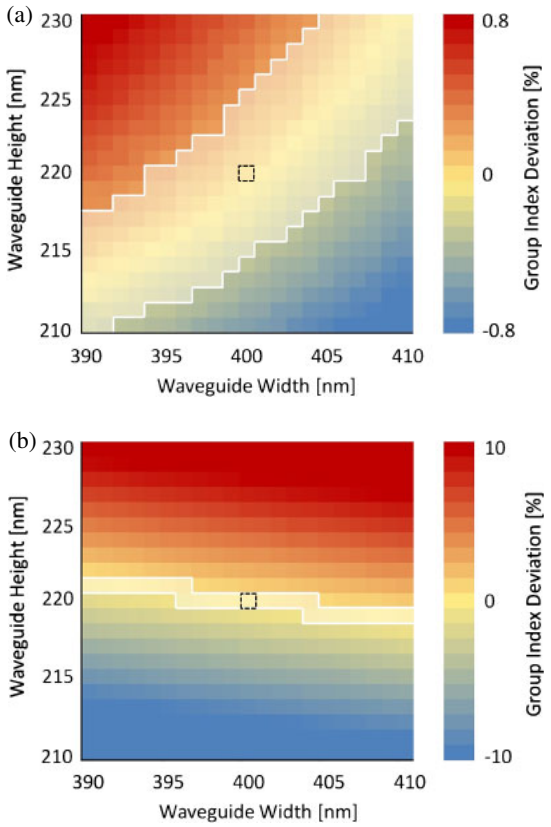

Fig. 7. (Color online) (a) Color map of n_g deviation from standard waveguide-core size 400 nm width × 220 nm height. The wavelength is about 1550 nm; and the polarization is in the TE-like mode. The waveguide-core size marked by a black broken line is 400 nm width × 220 nm height. The white meshed area corresponds to the n_g deviation measured from the ring resonators. (b) Color map of n_g deviation; polarization is in the TM-like mode.

from the n_g deviation of Si-wire waveguides. In this section, assuming that the estimated waveguide-core size distribution (width: 5 nm, height: 1 nm) arises from waveguides of any size, we calculated the relationship between the waveguide-core size and the waveguide properties. From the calculation results, we theoretically determined the waveguide-core size with a minimum device property distribution.

First, we calculated the n_{eff} of waveguides with various core sizes using FEM. The calculated core width was between 300 to 800 nm, and the calculated core height was between 40 to 300 nm, at a wavelength of 1550 nm and with polarization in the TE-like mode. Figure 8 shows a color map of the calculated n_{eff}. The high n_{eff} and strong light confinement effect are merits of the Si-wire waveguide. Therefore, having a high n_{eff} is a requirement for determining the core size of a waveguide. On the color map, the solid line from the upper left to the lower right shows the border of single-mode and multi mode operations. The waveguide-core sizes marked with circles are for Structure A, and the 540-nm-wide × 160-nm-high are for Structure B. The waveguide-core size of Structure A is standard, and we used it to estimate the waveguide-core size distribution in Sect. 2. The waveguide-core size of Structure B is the proposed optical waveguide-core size.

Figure 9 shows a color map of the n_{eff} distribution, in the case where the waveguide-core width is distributed within

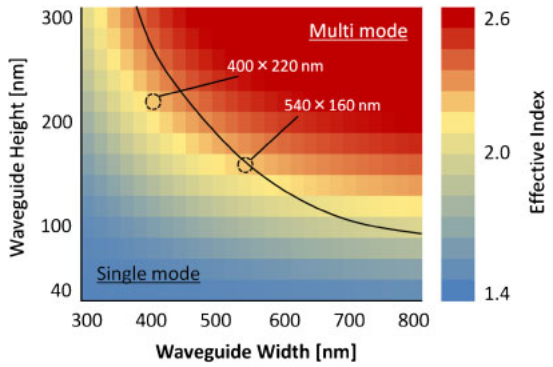

Fig. 8. (Color online) Color map of n_{eff} for waveguide-core widths of about 300 to 800 nm and waveguide-core height of about 40 to 300 nm. The calculated wavelength is 1550 nm; polarization is in the TE-like mode. The solid line on the color map is the border of the single-mode and multi-mode structures. The waveguide-core sizes marked by circles are 400 nm width × 220 nm height and 540 nm width × 160 nm height.

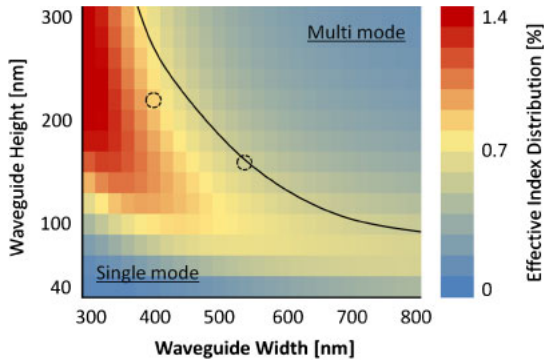

Fig. 9. (Color online) Color map of n_{eff} distribution.

5 nm, and the waveguide-core height is distributed within 1 nm. A smaller n_{eff} distribution of the Si-wire waveguide is needed to reduce the device property distribution. Summarizing these points, the required properties for the new core-size waveguide are as follows:

1. High n_{eff}
2. Small n_{eff} distribution caused by waveguide-core size distribution
3. Operation in single-mode at a wavelength of 1550 nm

We assumed that the ideal waveguide-core size falls along the single-mode line and has a small n_{eff} distribution. Figure 10 shows the n_{eff} distributions for various waveguide-core sizes along the single-mode line. The waveguide-core size having the smallest n_{eff} distribution was that of Structure B, and the n_{eff} distribution was 0.56%. This is because such a wide waveguide is not easily affected by waveguide-core width distribution. On the other hand, a thin waveguide is sensitive to the waveguide-core height distribution. We think that the n_{eff} distribution is mainly dominated by the width distribution in the range of less than 540 nm width and by the height distribution at a range of over 540 nm width. Because of these trade-off relations, we were able to determine the waveguide-core size with a minimum n_{eff} distribution and a high n_{eff}.

The transmission wavelength is an important device property of passive devices; it depends on n_{eff} and n_{g}. The

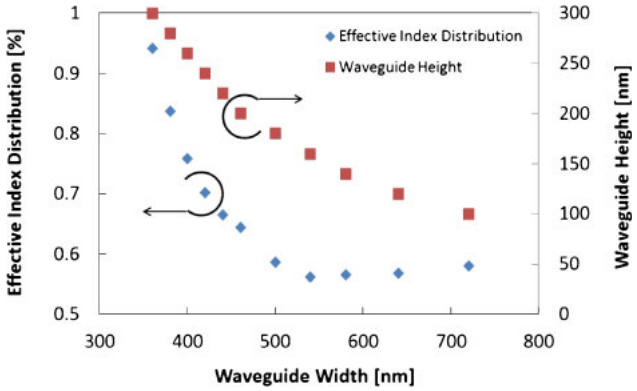

Fig. 10. (Color online) n_{eff} distribution along single-mode line.

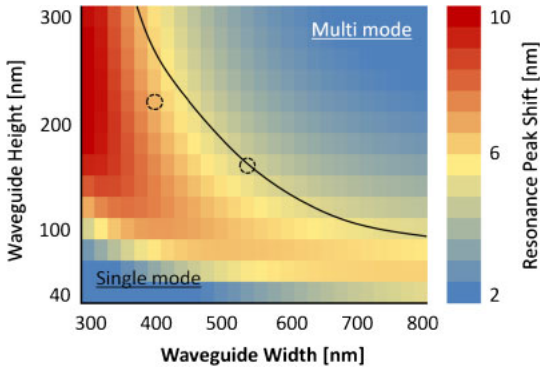

Fig. 11. (Color online) Color map of resonance peak shift of ring resonator. The standard wavelength is 1550 nm.

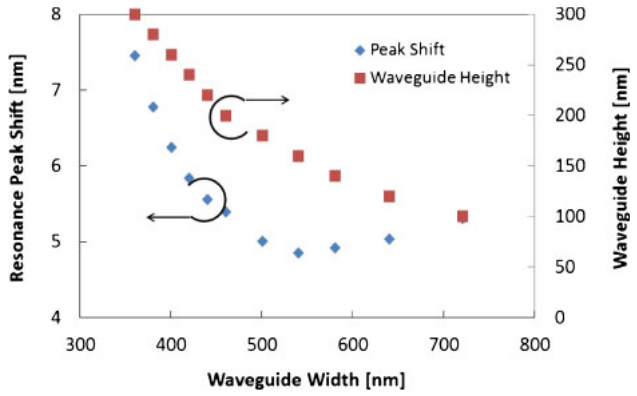

Fig. 12. (Color online) Resonance peak shift of waveguide-core size along single-mode line.

resonance peak shift of the ring resonator $\Delta\lambda$ can be calculated using

$$\Delta\lambda = \lambda \frac{\Delta n_{\mathrm{eff}}}{n_{\mathrm{g}}}, \tag{3}$$

where Δ denotes the deviation of the variable and λ is the standard wavelength of 1550 nm. Figure 11 shows the color map of the resonance peak shift caused by the n_{eff} distribution. Figure 12 shows the resonance peak shifts for various waveguide-core sizes along the single-mode line. The waveguide core size of Structure B had the smallest resonance peak shift of 4.86 nm. Considering not only n_{eff}

Table I. Calculated device properties of a selection of waveguide core sizes.

Core size (nm^2)	n_{eff}	n_{eff} distribution (%)	Resonance peak shift (nm)
400 × 220	2.22	0.85	6.68
440 × 220	2.31	0.66	5.56
540 × 160	2.22	0.56	4.86
720 × 100	1.95	0.58	5.30

but also device properties, this was the optimum core size. Table I shows the calculated device properties of a selection of waveguide core sizes, including Structures A and B. A wide waveguide such as the 440-nm-wide × 220-nm-high sample showed a high n_{eff}, but also a high n_{eff} distribution and resonance peak shift. Conversely, a thin waveguide such as the 720-nm-wide × 100-nm-high sample showed a comparatively low n_{eff} and a high resonance peak shift. With these observations in mind, we can assert that the optimization of the waveguide-core size can considerably reduce the device property distribution of Si-wire waveguide devices.

4. Conclusions

We fabricated Si-wire patterns and ring resonators on a 300 mm SOI wafer using the forefront CMOS-compatible process featuring ArF immersion lithography. The n_g deviation of the Si-wire waveguides at five different positions on the SOI wafer was examined by measuring the transmission spectra of the ring resonators. The measured n_{eff} deviations of group refractive indices were 0.3% for the TE-like mode and 1.1% for the TM-like mode. By comparing the measured n_g deviation and FEM calculation results, we estimated the waveguide-core size distribution for various Si-wire waveguides. The estimated maximum distribution of the waveguide-core width was 5 nm, and that of the waveguide-core height was 1 nm. Next, assuming that the estimated waveguide-core size distribution arises for waveguides of any core size, we calculated the n_{eff} distribution. From our calculations, the optimum waveguide core for reducing device property distribution was of 540 nm width and 160 nm height. In the case of this core size waveguide, the n_{eff} distribution caused by the waveguide-core size distribution was 0.56%. The resonance peak shift of ring resonators was also calculated to be 4.86 nm. These distributions were smaller than the device property distributions of current standard waveguide-core sizes such as 400 nm width × 220 nm height. We show that the property distribution of Si-wire waveguide devices can be reduced by the optimization of the waveguide-core size. Therefore, we can improve the device property uniformity of Si-wire waveguide devices, not only by improving the semiconductor process but also by optimizing the waveguide-core size.

Acknowledgments

This research was supported in part by the Strategic Information and Communications R&D Promotion Programme (142102003) from the Ministry of Internal Affairs and Communications. The device processing was conducted at the Super Cleanroom of the National Institute of Advanced Industrial Science and Technology (AIST), Japan.

1) R. Soref, IEEE J. Sel. Top. Quantum Electron. **12**, 1678 (2006).
2) B. Jalali and S. Fathpour, J. Lightwave Technol. **24**, 4600 (2006).
3) K. Wada, D. H. Ahn, D. R. Lim, J. Michel, and L. C. Kimerling, Thin Solid Films **508**, 418 (2006).
4) Z. M. Xu, M. Suzuki, Y. Tanushi, and S. Yokoyama, Appl. Phys. Lett. **88**, 161107 (2006).
5) Y. Tanushi and S. Yokoyama, Jpn. J. Appl. Phys. **45**, 3493 (2006).
6) Y. Amemiya, R. Furutani, M. Fukuyama, and S. Yokoyama, Jpn. J. Appl. Phys. **51**, 04DG07 (2012).
7) M. Nara, T. Kita, Y. Tanushi, and H. Yamada, Ext. Abstr. Solid State Devices and Materials, 2012, p. 540.
8) Y. Arakawa, T. Nakamura, Y. Urino, and T. Fujita, IEEE Commun. Mag. **51**, 72 (2013).
9) H. Yamada, T. Chu, S. Ishida, and Y. Arakawa, IEEE J. Sel. Top. Quantum Electron. **12**, 1371 (2006).
10) H. Yamada, T. Chu, S. Ishida, and Y. Arakawa, Appl. Phys. Lett. **86**, 191107 (2005).
11) K. Nemoto, T. Kita, and H. Yamada, Appl. Phys. Express **5**, 082701 (2012).
12) C. R. Doerr, N. K. Fontaine, and L. L. Buhl, IEEE Photonics Technol. Lett. **24**, 697 (2012).
13) T. Kita, K. Nemoto, and H. Yamada, Proc. IEEE Int. Conf. Group IV Photonics, 2013, p. 152.
14) T. Kita, K. Nemoto, and H. Yamada, J. Sel. Top. Quantum Electron. **20**, 8201806 (2014).
15) T. Kita, K. Nemoto, and H. Yamada, Jpn. J. Appl. Phys. **53**, 04EG04 (2014).
16) S. K. Selvaraja, G. Murdoch, A. Milenin, C. Delvaux, P. Ong, S. Pathak, D. Vermeulen, G. Sterckx, G. Winroth, P. Verheyen, G. Lepage, W. Bogaerts, R. Baets, J. Van Campenhout, and P. Absil, Proc. OECC, 2012, p. 15.
17) H. Takahashi, M. Toyama, M. Seki, D. Shimura, K. Koshino, N. Yokoyama, M. Ohtsuka, A. Sugiyama, E. Ishitsuka, T. Sano, and T. Horikawa, Ext. Abstr. Solid State Devices and Materials, 2012, p. 528.
18) H. Okayama, D. Shimura, H. Takahashi, M. Seki, M. Toyama, T. Sano, H. Yaegashi, T. Horikawa, and H. Sasaki, Electron. Lett. **48**, 869 (2012).
19) H. Okayama, D. Shimura, H. Takahashi, M. Seki, M. Toyama, T. Sano, K. Koshino, N. Yokoyama, M. Ohtsuka, A. Sugiyama, S. Ishitsuka, T. Tsuchizawa, H. Nishi, K. Yamada, H. Yaegashi, T. Horikawa, and H. Sasaki, Electron. Lett. **49**, 410 (2013).
20) T. Kita, Y. Tanushi, M. Nara, S. Hirano, M. Toyama, M. Seki, K. Koshino, N. Yokoyama, M. Ohtsuka, A. Sugiyama, E. Ishitsuka, T. Sano, T. Horikawa, and H. Yamada, IEICE Tech. Rep. OPE2013-7 (2013) [in Japanese].
21) Y. Tanushi, T. Kita, M. Toyama, M. Seki, K. Koshino, N. Yokoyama, M. Ohtsuka, A. Sugiyama, E. Ishitsuka, T. Sano, T. Horikawa, and H. Yamada, Proc. Int. Conf. Group IV Photonics, 2013, p. 105.
22) F. Boeuf, S. Cremer, N. Vulliet, T. Pinguet, A. Mekis, G. Masini, L. Verslegers, P. Sun, A. Ayazi, N.-K. Hon, S. Sahni, Y. Chi, B. Orlando, D. Ristoiu, A. Farcy, F. Leverd, L. Broussous, D. Pelissier-Tanon, C. Richard, L. Pinzelli, R. Beneyton, O. Gourhant, E. Gourvest, Y. Le-Friec, D. Monnier, P. Brun, M. Guillermet, D. Benoit, K. Haxaire, J. R. Manouvrier, S. Jan, H. Petiton, J. F. Carpentier, T. Quemerais, C. Durand, D. Gloria, M. Fourel, F. Battegay, Y. Sanchez, E. Batail, F. Baron, P. Delpech, L. Salager, P. De Dobbelaere, and B. Sautreuil, IEDM Tech. Dig., 2013, p. 353.
23) S.-H. Jeong, D. Shimura, T. Simoyama, M. Seki, N. Yokoyama, M. Ohtsuka, K. Koshino, T. Horikawa, Y. Tanaka, and K. Morito, Opt. Express **21**, 30163 (2013).
24) D. Marris-Morini, C. Baudot, J.-M. Fedeli, G. Rasigade, N. Vulliet, A. Souhaite, M. Ziebell, P. Rivallin, S. Olivier, P. Crozat, X. Le Roux, D. Bouville, S. Menezo, F. Boeuf, and L. Vivien, Opt. Express **21**, 22471 (2013).
25) S. K. Selvaraja, W. Bogaerts, P. Dumon, D. Van Thourhout, and R. Baets, IEEE J. Sel. Top. Quantum Electron. **16**, 316 (2010).
26) H. Tian, G. Winzer, K. Petermann, B. Tillack, and L. Zimmermann, J. Eur. Opt. Soc. Rapid Publ. **7**, 12032 (2012).
27) T. Baehr-Jones, R. Ding, A. Ayazi, T. Pinguet, M. Streshinsky, N. Harris, J. Li, L. He, M. Gould, Y. Zhang, A. E.-J. Lim, T.-Y. Liow, S. H.-G. Teo, G.-Q. Lo, and M. Hochberg, arXiv:1203.0767.
28) D.-X. Xu, J. H. Schmid, G. T. Reed, G. Z. Mashanovich, D. J. Thomson, M. Nedeljkovic, X. Chen, D. Ven Thourhout, S. Keyvaninia, and S. K. Selvaraja, IEEE J. Sel. Top. Quantum Electron. **20**, 8100217 (2014).
29) D. G. Seiler, S. Zollner, A. C. Diebold, and P. M. Amirtharaj, in *Handbook of Optics*, ed. M. Bass (McGraw-Hill, New York, 2009) 3rd ed., Vol. 4, Chap. 5.
30) Y. Atsumi, D.-X. Xu, A. Delage, J. H. Schmid, M. Vachon, P. Cheben, S. Janz, N. Nishiyama, and S. Arai, Opt. Express **20**, 26969 (2012).